Elastomeric Polymers. 2. NMR and NMR Imaging Characterization of Cross-Linked PDMS

Maristella Gussoni,*,† Fulvia Greco,‡ Marina Mapelli,§ Alessandra Vezzoli,⊥ Elisabetta Ranucci,# Paolo Ferruti,# and Lucia Zetta‡

Dipartimento di Scienze e Tecnologie Biomediche, Università di Milano, Milano, Italy; Istituto di Chimica delle Macromolecole, CNR, Milano, Italy; Istituto Oncologico Europeo, Milano, Italy; Ex Istituto di Tecnologie Biomediche Avanzate, CNR, Milano, Italy; and Dipartimento di Chimica Organica e Industriale, Università di Milano, Milano, Italy

Received July 30, 2001

ABSTRACT: Proton NMR relaxometry and imaging have been applied to investigate the molecular properties of silicone rubber networks unfilled, filled with silica, washed from the sol component, and in the presence of a guest polymer. For all the analyzed samples, the decay of the echo magnetization has been discussed on the basis of a single chain model with a distribution of dipolar interactions. The relaxation parameters have been investigated in order to correlate the structural and motional parameters of the elastomeric networks to the macroscopic characteristics of materials, mainly the cross-link density. On test samples a quite good agreement has been found between the calculated cross-link density and the T_2 and the qM_2 residual dipolar coupling parameters, determined by fitting the transverse magnetization decay on the basis of the assumed chain model. The imaging technique has been employed to characterize two networks, endowed with intrinsically different chain mobility and characterized by the presence and the absence of silica filler. An "in situ" polymerization reaction occurring in the silicones has been followed by NMR relaxometry and imaging techniques. The effects of thermal and chemical processes on the two different elastomeric matrices as well as the quality of the distribution of the guest polymer inside the host matrix have been assessed.

1. Introduction

Nuclear magnetic resonance imaging (NMRI) is up to now a widely accepted tool for nondestructive mapping of spatial structures in materials.[1−4] On the other hand, NMR spectroscopy (NMRS) is very sensitive to chemical composition and molecular structure of a sample, particularly through relaxation parameters. However, materials are characterized by relaxation decays with rates differing by several orders of magnitude. The proton response in the crystalline region decays with a spin−spin relaxation time, T_2, of about 10^{-5} s, whereas the T_2 from nuclei in the amorphous region has values ranging from 10^{-2} to 1 s.[5] Therefore, crystalline materials require experimentally demanding line-narrowing methods in conjunction with spectroscopic and imaging techniques.[6] In the latter case a drastic reduction in TE, as may be achieved by strong gradients and fast digitizers, is mandatory to obtain T_2 independent images of most common filled elastomers. In the case of amorphous chain units the behavior of the transversal relaxation time, T_2, is quite complex, as expected on the basis of extensive studies.[7−19] The transversal magnetization decay is generally associated with the low-frequency motions of large portions of a polymer; therefore, it is very sensitive to any factor affecting the molecular mobility, such as the presence of free polymer chains, cross-links, or fillers.

Silicones are most suitable polymers for both NMRS and NMRI studies. They are rich in protons, the most sensitive NMR nucleus, and their elastic properties derive from high molecular mobility in combination with form stability. Their macroscopic properties can range from those of viscous liquids to those of rigid solids by changing the cross-link density and the filler concentration. Their glass transition temperature is well below room temperature (ranging from −120 to −60 °C); therefore, typical proton NMR line widths for such materials at about 100 °C above T_g are in the range 100−2000 Hz. Molecular mobility averages the spin dipolar interactions significantly from the rigid case, resulting in proton T_2's typically in the range of milliseconds, suitable for high-resolution spectroscopy and imaging by standard techniques.[20]

In our previous paper,[21] we studied a commercial silicone rubber by spin-echo and gradient-echo NMRI techniques. The swelling process in different solvents was analyzed, different kinds of inhomogeneities were localized, and the commercial silicone was used as a matrix for an "in situ" polymerization reaction suitable for biomedical application. The present paper reports the application of NMRS and NMRI techniques to the study of different silicone rubber networks. Particular attention has been given to molecular dynamics, as measured through nuclear relaxation times by NMRS, and to the spatial localization of elastomeric properties, studied by NMRI. Three different kinds of silicones have been analyzed: (i) synthetic silicones without silica filler and with a known chemical composition of the network (SILNS); (ii) a commercial silicone with silica filler, endowed with an elastomeric matrix, whose cross-link type and density were not known (SILS); and (iii) SILS extracted with an organic solvent (SILV).

† Dipartimento di Scienze e Tecnologie Biomediche, Università di Milano.
‡ Istituto di Chimica delle Macromolecole, CNR.
§ Istituto Oncologico Europeo.
⊥ Ex Istituto di Tecnologie Biomediche Avanzate, CNR.
Dipartimento di Chimica Organica e Industriale, Università di Milano.
* Corresponding author: e-mail Maristella.Gussoni@unimi.it; Fax +39-2-7064-3557.

10.1021/ma011356d CCC: $22.00
Published on Web 02/01/2002

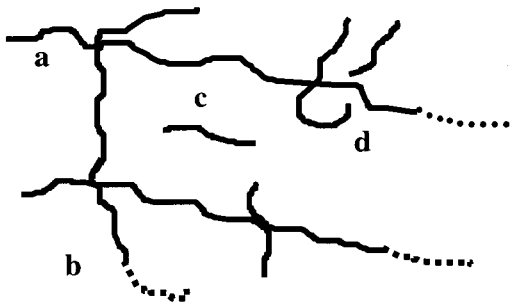

Figure 1. Schematical representation of the different mobile molecular parts in an elastomeric network: (a) inter-cross-linked chain, (b) dangling chain end, (c) free chain (sol part), (d) physical loop (entanglement).

The main results of this study are (i) the characterization of elastomeric properties, in particular the chain mobility, of all silicone matrices endowed with different networks, in the presence or in the absence of silica filler and in the presence of a guest polymer, as assessed by the relaxation parameters and from the image contrast; (ii) the correlation on the synthesized samples between the structural and motional NMR parameters and the theoretical characterization of the elastomeric network, mainly the cross-link density; and (iii) the direct assessment of effect of an "in situ" polymerization reaction on two different matrices characterized by the presence and the absence of a silica filler.

2. Theory

It is well-known that the T_2 decay curves of cross-linked elastomers are not exponential. The interpretation of this behavior in terms of structural parameters used in the present paper was based on a modified single chain model[9−12] which has been previously described[13,14] and successfully tested. The model has been applied to study by NMRS measurements the transversal relaxation times in rubber samples with well-known cross-link density[13] and to investigate by NMRI the material properties of differently cross-linked and carbon-black-filled elastomers.[15−17] The same model was largely applied to characterize the aging process in carbon-black-filled natural rubbers, silica, and carbon-black-filled SBR as well as milled rubbers.[22,23] It was also employed to investigate the swelling behavior of rubber networks.[24,25]

According to the model, network chains are assumed to be "noninteracting Kuhn chains",[26] consisting of freely joined statistical segments. The scheme in Figure 1 illustrates the principal mobile parts in a rubber network. Namely, they are the following:

(i) "Inter-cross-link chains" fixed at both ends and endowed with two relaxation mechanisms. The first consists of a local motion, very fast ($\tau_{fast} = 10^{-8}$ s) compared to the operative NMR time scale ($1/\nu_H \approx 10^{-6}$ s) of the dipolar interaction associated with a pair of protons. Thus, a small residual part of the dipolar interaction remains, and it is expressed as the ratio q of the second moment M_2^{Res} in the material (that represents the residual interaction which is not averaged by the fast motion) and the second moment M_2 (1.23×10^{10} s^{-2}) in a rigid lattice.[27] For segments of inter-cross-link chains q typically assumes values of order of 10^{-4}. Because of the large size of this moving object, the correlation time τ_{slow} is on the order of 10^{-3} s.

(ii) "Dangling chain ends" fixed only at one side. Their segmental fast motion ($\tau_{fast} = 10^{-8}$ s) is nearly isotropic ($q \approx 0$).

(iii) "Physical loops" (entanglements) which lead to a decrease in molecular mobility due to an impairment of the freedom degree.

(iv) "Free chains" , the so-called sol part, characterized by an isotropic motion and showing a liquidlike behavior. The long exponential decay of this fraction ($C \exp(-t/T_{2,\,sol})$) has not been considered in the present study. In fact, before fitting our experimental data, this slow component, still present in the FID after a time longer than 100 ms, was optionally removed by the program.

Therefore, the total transversal magnetization decay is composed of the first three aforementioned contributions and, according to the simplified version by Kuhn et al.,[15] is given by

$$M(t) = A \exp(-t/T_2 - qM_2t^2/2) + B \exp(-t/T_2) \quad (1)$$

where the fractions A and B represent the part of proton magnetization of cross-links and dangling chain ends, respectively, q is the anisotropy parameter, sensitive to both chemical cross-links and entanglements, M_2 is the second moment of the dipolar interaction in a rigid lattice, T_2 is the transversal relaxation time, and $M(t)$ is the magnetization decay (see Figure 2).

3. Experimental Section

3.1. Materials. The study was carried out on different silicone samples. The first series of test samples, synthesized in our laboratory, consisted of four unfilled silicones (SILNS) referred to as C, P, N, and H, endowed with a different elastomeric matrix. The samples were obtained by mixing known amounts of two oligomers represented in Scheme 1. The relative amounts (g/g) of the two reagents are reported in Table 1**.** The cross-linking reaction, leading to the tridimensional silicone rubber network, is shown in Scheme 1. It proceeds via an addition reaction between the hydrosilane group Si−H present in oligomer II and the terminal vinyl groups present in oligomer I, the cross-linking agent. The addition reaction is catalyzed in the presence of a platinum(II) complex, namely dichlorocyclooctadieneplatinum(II). The reaction mixture was poured into a Petri dish and left reacting for 24 h at room temperature without mixing. Scheme 1 also reports the molecular weight (M_W) of each oligomer; the number and the molecular weight of the repetition units (M_{WRU}) forming a single chain of both oligomer I and oligomer II. SILNS samples were sliced into small cylinders with an approximate height of 2 mm and a diameter of 8 mm.

Another sample (SILS) consisted of a commercial silicone rubber, Silopren HV, purchased from Bayer. SILS is cured, filled with silica up to 40−50%, endowed with a density of 1.0−1.2 g cm^{-3}, and thermally stable at temperatures higher than 350 °C. It contains vinyl groups, and its elemental analysis corresponds to the structure $[SiMe_2-O]_n$.

To remove unreacted siloxanes, a few SILS samples were extracted for several days with toluene at 90 °C and then deswollen with toluene−methanol mixtures of increasing methanol fraction content (SILV).

SILS and SILNS-P samples were selected as matrices for an "in situ" polymerization reaction, directly induced in the NMR tube under nitrogen. The whole polymerization procedure has been described in previous papers.[28−31]

3.2. NMRS and NMRI Methods. All NMR experiments were carried out on a 4.7 T Bruker AM WB spectrometer equipped with a probehead tunable at the ^{1}H resonance frequency (200.13 MHz) and a gradient drive unit utilized for NMRI experiments. More information on the experimental apparatus is reported in our previous paper.[21] All experiments were carried out using a 15 mm insert. The sample was

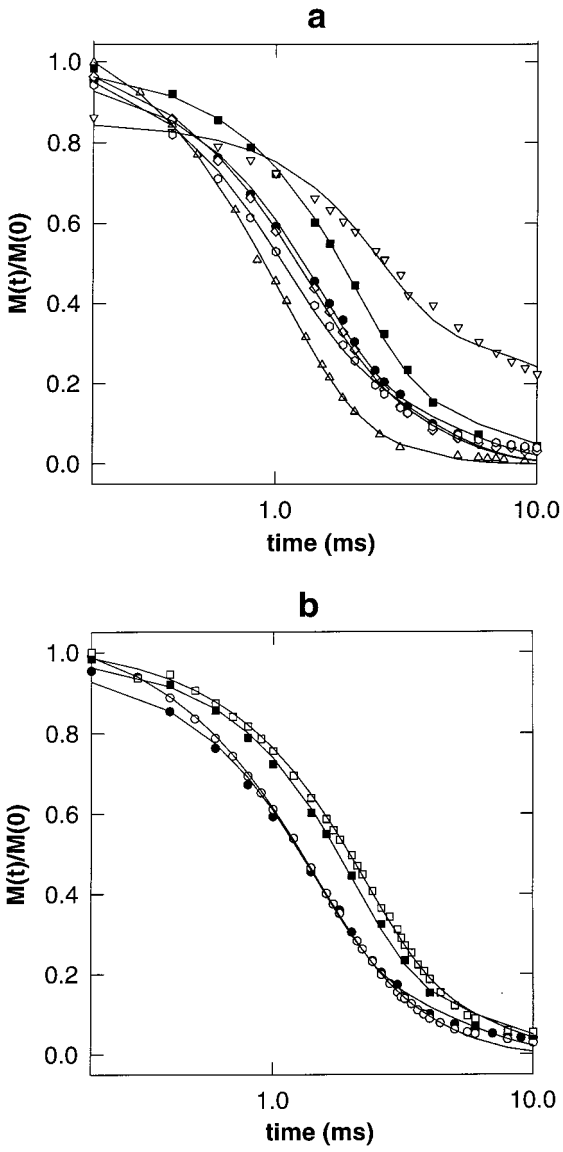

Figure 2. Measured (symbols) and fitted (solid lines) relaxation curves of the transversal magnetization decay $M(t)$ vs the echo time ($t = 2\tau$ of the Hahn spin-echo sequence) of (a) SILNS: C (▽), N (◇), H (○), P (●); SILS (■) and SILV (△) samples, and (b) SILS and SILNS (P) before (filled symbols) and after (open symbols) the "in situ" polymerization reaction.

introduced into a 10 mm NMR tube. A phase/frequency encoding 2D imaging spin-echo sequence, standardly supplied by Bruker, was employed. 512 × 512 matrices were acquired with 300 averages and a voxel resolution of 43 × 43 × 2000 μm^3, obtaining the images in about 8 h. The acquisition parameters were spectral width of 100 kHz, echo delay time (TE) ranging from 12 to 18 ms, and recycle time (TR) of 1 s. Thus, all images were T_1 weighted in the same way and differently T_2 weighted. Selective rf pulses (2000 Hz bandwidth, Gaussian-shaped, truncated at 5% level) were used. Other acquisition parameters are reported in the figure captions.

Bulk ^{1}H NMRS T_1 and T_2 measurements were carried out using inversion−recovery (IR) and Hahn spin-echo sequences, respectively. The inversion recovery time in IR sequence was varied between 500 μs and 5 s (number of experiments NE = 25). The echo time (TE between the 90° rf and the center of the echo) in spin-echo sequence ranged from 50 μs to 10 s (NE = 50). The repetition time, TR, was 20 s in both cases, i.e., 5 times longer than T_1. Longitudinal relaxation times values were calculated with the supplied DISR89 Bruker software. The Gauss-like relaxation function of the magnetization decay was fitted using eq 1 (see Theory section). Experimental data were fitted by the Marquardt−Levenberg algorithm implemented by the Sigma Plot software (Jandel).

Effective spin−spin relaxation times (T_2*) were determined from the signal line width in a standard FT spectrum ($T_2^* = 1/\pi\Delta\nu_{1/2}$, where $\Delta\nu_{1/2}$ is the width at half-height of the individual peak) as

$$\Delta\nu_{1/2,\mathrm{SILNS}} = 434 \text{ Hz at } 25\ ^\circ\mathrm{C}$$

$$\Delta\nu_{1/2,\mathrm{SILS}} = 219 \text{ Hz at } 25^\circ\mathrm{C}$$

4. Results and Discussion

4.1. Magnetization Decay and Material Parameters. 4.1.1. Unfilled Samples. To estimate the different structure of the SILNS networks, mainly in terms of cross-link density, it was assumed that the cross-linking reaction, which is the addition reaction between Si−H groups present in oligomer II and terminal vinyl groups present in oligomer I (see Scheme 1), does reach the 100% yield. Table 1 reports the number of reacting functional groups of both oligomer I and oligomer II forming cross-links. As reported in the table, they were calculated starting from the relative amounts of the two reagents, mixed to synthesize the samples. It can be observed that for all samples oligomer II presents more reactive functional groups than oligomer I. In fact, the reactive functions calculated for oligomer I, the cross-linking agent, range from 1.5×10^{-3} for H sample to 3.74×10^{-4} for C sample. On the other hand, the reactive functions calculated for oligomer II range from 8×10^{-3} for C and H samples to 2.56×10^{-3} for the P sample. Moreover, the terminal ends of the oligomer II are not reactive, while those of oligomer I are all reactive (see Scheme 1). Therefore, the following can be concluded: (i) terminal ends of oligomer I are never constrained to chain segments; (ii) all Si−H functions react forming constraints. By defining A_{th} as the total number of chain segments fixed at both ends, namely the cross-link density, it can be calculated as

$$A_{\mathrm{th}} = N_{\mathrm{I}} + N_{\mathrm{const,II}} \tag{2}$$

where N_{I} is the number of molecules of oligomer I, corresponding to the chain segments fixed at both ends of oligomer I, and $N_{\mathrm{const,II}}$ is the number of constrained segments present in the chains of the oligomer II. In fact, all moles of oligomer I react at both ends, giving an equivalent number of constrained segments. On the other hand, $N_{\mathrm{const,II}}$ can be calculated as

$$N_{\mathrm{const,II}} = (N_{\mathrm{NET}} - 1)N_{\mathrm{II}} \tag{3}$$

where N_{II} is the number of molecules of oligomer II and N_{NET} is the mean number of cross-links in a single chain of oligomer II, which is

$$N_{\mathrm{NET}} = 2N_{\mathrm{I}}/N_{\mathrm{II}} \tag{4}$$

Therefore, $N_{\mathrm{NET}} - 1$ is the number of chain segments. N_{I}, N_{NET}, $N_{\mathrm{const,II}}$, and A_{th} parameters calculated by using eqs 2−4 are reported in Table 2 for all SILNS samples. As regards sample C, it can be pointed out that only one chain of oligomer II is joined to oligomer I, that is, about 50% chains of oligomer II can neither react nor be constrained to any end. Thus, the A_{th} value calculated for C sample is negative. On the other hand, the maximum A_{th} corresponds to sample H, which means the most cross-linked network, since it contains

Scheme 1. Cross-Linking Reaction of Unfilled Samples

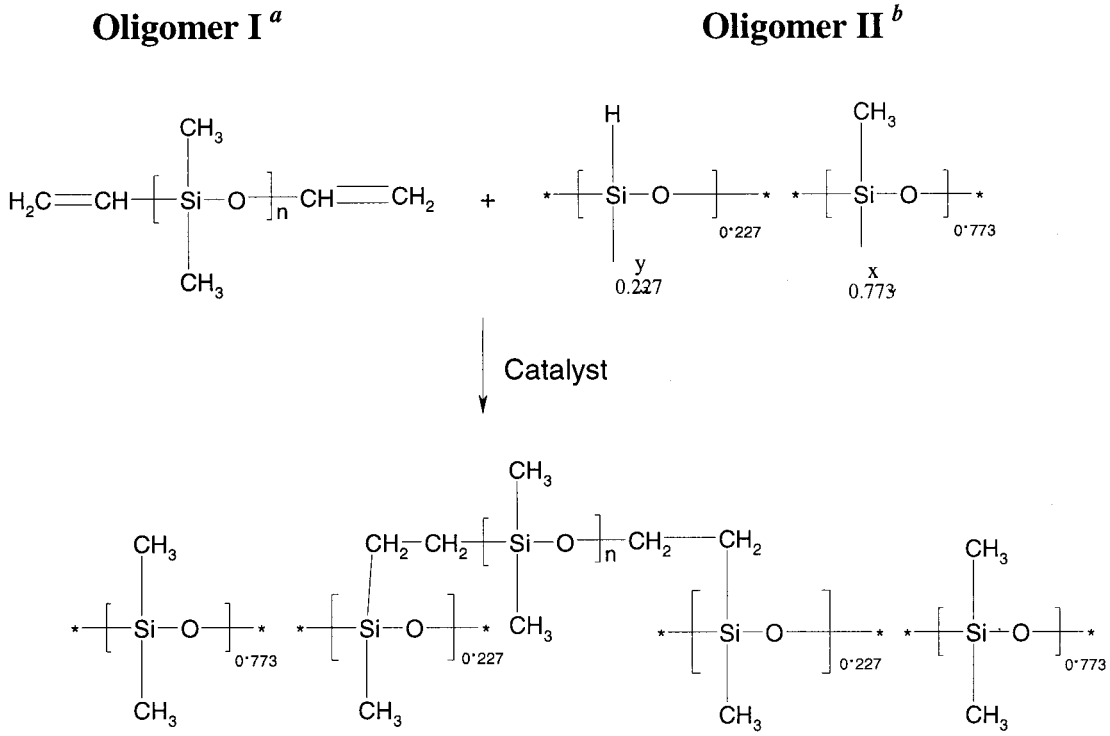

[a] I: $(n = 132)$; $M_w = 10\,000$; $M_{WRU} = 74.156$. [b] II: $(x + y) = 24$; $M_W = 3000$; $M_{WRU} = 60.156 \times 0.227 + 74.156 \times 0.773 = 70.94$.

Table 1. Number of Reactive Functional Groups of Oligomer I[a] and II[b]

			no. reactive functional groups	
sample	oligomer I (g)	oligomer II (g)	oligomer I $(\times 1/N_{AV})$[c]	oligomer II (N_{Si-H}) $(\times 1/N_{AV})$
C	1.87	2.5	3.74×10^{-4}	8.00×10^{-3}
H	7.50	2.5	1.50×10^{-3}	8.00×10^{-3}
N	4.50	0.5	9.00×10^{-4}	1.60×10^{-3}
P	4.00	0.8	8.00×10^{-4}	2.56×10^{-3}

[a] Number of reactive functional groups oligomer $I = 2 \times$ oligomer I moles $\times N_{AV}$. [b] Number of reactive functional groups oligomer II $= N_{Si-H} = N_{RU} \times 0.227 \times N_{AV}$; N_{RU} = g of polymer/M_{WRU}. [c] N_{AV} = (Avogadro number) 6.0225×10^{23} molecules/mol.

Table 2. Calculation of A_{th} Values

sample	N_I $(\times 1/N_{AV})$	N_{NET}	$N_{const,II}$	A_{th} $(\times 1/N_{AV})$
C	1.87×10^{-4}	0.4490		
H	7.50×10^{-4}	1.8007	6.6698×10^{-4}	1.4170×10^{-3}
N	4.50×10^{-4}	5.3892	7.3300×10^{-4}	1.1830×10^{-3}
P	4.00×10^{-4}	2.9962	5.3298×10^{-4}	9.3300×10^{-4}

the maximum number of active functions of oligomer I. In fact, SiH groups are always more than the reactive functions of oligomer I; therefore, the probability of forming cross-links mainly depends on the amount of oligomer I reactive functions. On the other hand, calculations are made assuming a 100% yield of the reaction; therefore, higher A_{th} values indicate a more cross-linked network. In conclusion, by putting the samples in order of increasing cross-linked network, we find sample C, sample P, sample N, and sample H.

Figure 2a shows the decay of the proton transversal magnetization vs the echo time for all the investigated networks (symbols), after subtraction of the sol contribution, and the fitted curves (continuous lines) obtained using eq 1 of the Theory section. The typical magnetization decay of elastomers in a Hahn spin-echo experiment can be observed, in particular the clear nonexponential beginning of all curves. Despite the difference among the curves relative to each sample, the correspondence between experimental data and fitted curves is excellent in all cases. The magnetization decay follows a similar behavior for N (◇), H (⬡), and P (●) samples. On the contrary, the sample C (▽) shows a quite different behavior. Its magnetization is still at about the 40% of the initial value after 10 ms.

The nonexponential magnetization decay was not properly describable by the single parameter T_2. According to the model chosen to describe the elastomeric network, other independent parameters, related to the network structure, could be obtained from the statistical analysis of the fit curves. The results obtained fitting eq 1 to the experimental magnetization decays are summarized in Table 3. In particular, the values of the parameters T_2 and qM_2 can be compared to the number of reactive functions calculated for oligomer II and reported in Table 1 as well as to the A_{th} values reported in Table 2. It can be observed that as the reactive functions increase, that is, when increasing the probability of forming cross-links, the qM_2 anisotropy value becomes higher and the corresponding T_2 value becomes lower. Both findings indicate an increased rigidity of the network structure. As well, A_{th} values, calculated assuming a 100% yield of the reaction, indicate sample C endowed with the least cross-linked network and sample H as the most rigid. Both T_2 and qM_2 values obtained by fitting the experimental data lead to the same conclusions. Therefore, on the basis on the adopted single chain model, the structures of the networks of all SILNS samples result in accord with the theoretically determined structures. Indeed, an important topic in the field of polymeric network is the quantitative correlation between qM_2 and the cross-link density. This figure is widely reported in the literature, in particular in studies on vulcanized industrial SBR elastomers[18] as

Table 3. Relaxation Parameters for All Samples

	unfilled				filled		in situ polymerized	
sample	C	P (SILNS)	N	H	SILS	SILV	SILNS	SILS
$B/(A+B)$, %	54 (6.2)[a]	63 (13)	51 (14.7)	48 (18.2)	72 (12.4)	69 (9.8)	49 (10.8)	63 (10.6)
qM_2,[b] ms^{-2}	0.30 (8.5)	0.69 (8.3)	0.72 (12)	1.32 (14.6)	0.37 (8.5)	0.84 (14.1)	0.56 (8.5)	0.26 (7.4)
T_2, ms	20.60 (8.3)	3.57 (10.6)	2.37 (7.8)	2.41 (10.9)	5.71 (12.9)	1.49 (8)	2.26 (5)	4.42 (6.3)
T_1, s (mean value)	1.067 (0.21)				1.061 (0.23)			

[a] The numbers in parentheses represent the coefficients of variation, expressed as a percentage. [b] $M_2 = 1.23 \times 10^{10}$ s^{-2} (see section 2).

well as on differently vulcanized natural rubber samples.[19] A $qM_2 < 1$ ms^{-2} was considered always fulfilled for weakly cross-linked samples, whereas $qM_2 > 1$ ms^{-2} was ascribed to highly cross-linked samples.[19] In the present study the possibility of establishing an absolute quantitative correlation between the theoretically calculated cross-links, A_{th}, and the cross-link density measured by qM_2 parameters, fitted by NMR data, was limited by the impossibility of (i) separating the contribution of physical and chemical cross-links and (ii) establishing the real yield of the vulcanization reaction. In fact, our q values represent the contribution of the densities of both physical (q_0M_2), that is, entanglements, and chemical cross-links, which we could not separately measure. Nevertheless, our data clearly show that, when theoretical cross-link density increases (see A_{th} values of Table 2), qM_2 values increase too, even if it is impossible to identify a trend, due to the aforementioned limitations and the few samples. Nevertheless, we can surely state that qM_2, being the NMR parameter which reflects the effect of residual dipolar interactions, is the most sensitive to cross-link density. Sample C results a borderline case, since it shows a quite long T_2 (20.6 ms) and the lowest qM_2 (0.30) Accordingly, this sample has the lowest number of reactive functions so that A_{th} calculated value was unacceptable.

Table 3 also reports the percentage of the magnetization decay that can be related to the dangling chain ends (parameter $B/(A+B)$). Nevertheless, this parameter did not show a significant tendency. Despite the increasing amount of the active functions of oligomer I, the content of dangling chain ends seemed to keep rather constant. On the other hand, on the basis of the experience collected on a great number of elastomeric materials, it is well-known that while the parameter qM_2 is the most stable and reproducible one, the A and B parameters are not always in accordance with the expectation.[14−17]

The longitudinal relaxation times, T_1's, were analyzed assuming a single-exponential recovery as a reasonable relaxation model. The values measured on all SILNS samples were not found significantly different; thus, only the mean value of T_1 calculated among all SILNS and its standard deviation are reported in Table 3.

4.1.2. Silica-Filled Samples. As reported in Figure 2a, the relaxation decay of sample SILS (■) is at an intermediate position between the decay of sample C and that of samples H, P, and N. The SILV relaxation decay (△) appears very fast, its magnetization being negligible after about 3 ms. The curves (continuous lines) show a very good fit to the experimental data, indicating that also these elastomeric matrices, different in composition from the previous ones and filled with silica, could be well described by a single chain model. The fitting parameters reported in Table 3 indicate that sample SILS, endowed with a different elastomeric network, shows an intermediate behavior when compared with the SILNS samples. Its T_2 value is longer than those of N, H, and P samples, while the qM_2 anisotropic parameter is similar to that of sample C. The SILV sample, obtained from SILS after a washing procedure, shows a quite rigid network structure as indicated by its fast magnetization decay and by the T_2, which is the shortest T_2 value reported in the table. The sol molecules, as unreacted chains or admixtures of high mobility, were mainly eliminated by the extraction procedure. However, a higher qM_2 value (0.84) is found for SILV with respect to SILS (0.37), while qM_2 should not be changed upon the extraction procedure. Most likely, the high temperature used for the extraction process induced additional cross-links due to an accelerated oxidative aging process affecting both T_2 and qM_2. This finding suggested us to use temperature conditions as soft as possible and nitrogen atmosphere during the "in situ" polymerization, to avoid fast aging.

The longitudinal relaxation times did not significantly differ for SILS and SILV; thus, only the mean value of T_1 and its standard deviation are reported in Table 3. Moreover, these T_1's were found quite similar to those of the SILNS samples; hence, it could be concluded that the T_1 relaxation parameter is not significantly affected either by the presence of silica or by cross-links, host polymers, or sol molecules.

4.2. NMR Imaging. It is well-known that spectroscopic relaxation data give information which are averaged on the whole sample, while images provide a knowledge of the spatial distribution of material properties. Hence, a combination of NMRS and NMRI techniques was used to better characterize some of the SILS and SILNS silicone systems described above.

NMRI spin-echo experiments were performed on SILS and SILNS P samples. The P sample was chosen as endowed with an elastomeric network cross-linked at an intermediate level. Figure 3 shows the T_2-weighted images collected on the two pieces of silicones located into the same NMR tube: SILS (arrowed) on the left and SILNS P on the right side, imaged at echo times (TE) of (a) 12.0, (b) 14.0, (c) 15.5, and (d) 18.0 ms. These samples were previously used for the NMRS experiments (see section 4.1.2). Indeed, because of the long dead time of our instrumentation, mainly deriving from the gradient stabilization delay (1 ms), all images were collected using echo times (from 12.0 to 18.0 ms) long if compared to the spin−spin relaxation times of the two silicones (3.57 ms for SILNS P and 5.71 ms for SILS; see Table 3) but still short enough to have high spatially resolved images (43×43 μm^2). At any echo time the image contrast of sample SILS results brighter than that of sample SILNS. Using an echo time of 15.5 ms (Figure 3c), the sample SILS gives much more proton signal than the sample SILNS, while at an echo time of 18 ms (Figure 3d) no signal can be detected for sample SILNS, whereas SILS is still slightly visible. These features suggest that the SILS network was endowed with higher chain mobility, despite the presence of the silica filler. Moreover, the images of the two pieces of silicones appear mostly homogeneous, indicating, mainly

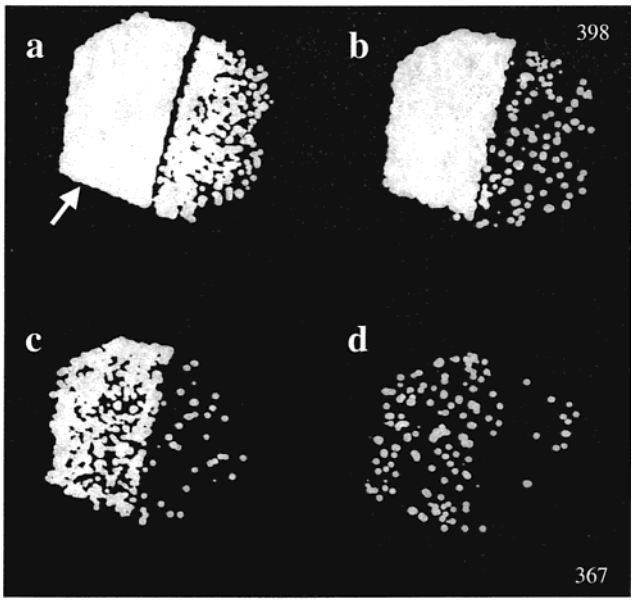

Figure 3. T_2-weighted spin-echo images of a piece of SILS (left, arrowed) and SILNS (right). Acquisition parameters: TE: (a) 12.0, (b) 14.0, (c) 15.5, and (d) 18.0 ms; *xy*-field of view (FOV): 11 mm; voxel resolution: $43 \times 43 \times 2000$ μm^3; RG = 200; NE = 300.

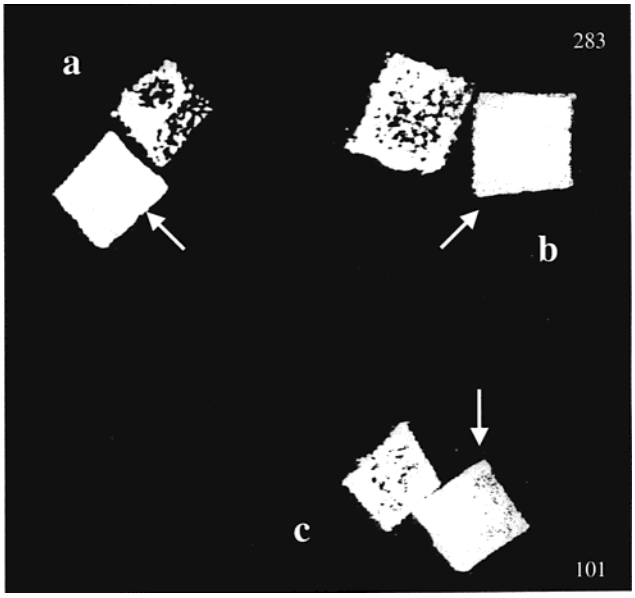

Figure 4. Spin-echo images acquired during the "in situ" polymerization process performed on SILS (indicated by an arrow) and SILNS samples: (a) image at room temperature, as a reference; (b) image at 0 °C after swelling the silicones with perdeuterated toluene; (c) image at room temperature after the polymerization reaction. Acquisition parameters: *xy*-field of view (FOV): 11 mm; voxel resolution: $43 \times 43 \times 2000$ μm^3; RG = 200; NE = 300.

at the shortest echo time (Figure 3a), the absence of any possible source of inhomogeneities such as voids, defects, large agglomerates of silica, or regions endowed with significantly different mobility. Unfortunately, gradient echo images, more sensitive to inhomogeneities, caused by differences in susceptivity, could not be obtained at this spatial resolution.

SILV did not give images at the chosen resolution, in accordance with its very fast echo-magnetization decay (Figure 2a) that gave a short T_2 value and a high qM_2 (see Table 3).

4.4. "In Situ" Polymerization. In our previous paper,[21] an "in situ" polymerization reaction was induced on a SILS sample and followed by NMRI spin-echo and gradient-echo experiments. Before the reaction, the SILS matrix, whose composition and cross-linking degree were unknown, was characterized, defects and inhomogeneities were detected, and the swelling process by toluene was described. The study assessed that the polymerization reaction did not significantly alter the properties of the elastomeric matrix and that the guest polymer did not form large agglomerates at the spatial resolution used for imaging.

With the aim of studying the effect of the polymerization reaction on samples containing or not silica filler, the two samples SILS and SILNS P, previously characterized by NMRS (Figure 2b) and NMRI (Figure 3), were employed. The main goal was to separate the rigidifying effect of silica from that of the polymer. The two samples were put in the same NMR tube, and the reaction was studied by using both NMRS and NMRI techniques.

4.4.1. Relaxation Parameters. Figure 2b shows the transversal magnetization decay for both SILS and SILNS before (full symbols) and after (open symbols) the "in situ" polymerization and the curves (continuous lines) fitting the experimental data. The magnetization decay, particularly the Gauss-like shape of the initial part, could be well fit by a single chain model both before (data shown also in Figure 2a) and after the polymerization process. The decays of the two samples are significantly different, while no substantial difference appears between the decays collected before and after the reaction. The relaxation parameters, calculated by fitting the data with eq 1, are summarized in Table 3. The T_2 relaxation times are slightly shortened when the guest component is present in the matrix (SILNS: 3.57 and 2.26 ms; SILS: 5.71 and 4.42 ms), while the fraction of the second moment, qM_2, affected by both cross-link density and entanglements, remains practically unchanged.

T_1 values do not significantly change upon polymerization.

4.4.2. NMR Imaging. As reported in our previous paper,[21] the swelling properties studied on SILS indicated that toluene was a good solvent to swell silicones and to dissolve the monomeric mixture selected for the "in situ" polymerization. The SILS and SILNS samples were cut in smaller pieces to allow them to suitably enlarge in the NMR tube. Then, the polymerization reaction was carried out at the same time and under identical experimental conditions for the two elastomers.

The reaction process was followed by imaging all steps of the polymerization, keeping the same NMRI acquisition parameters, to be able to compare each phase of the process and to rationalize any possible change in light and dark contrasts. Figure 4 shows the spin-echo images collected on the two bars of SILS (arrowhead) and SILNS P at three different stages. An image was collected at room temperature, before the onset of the "in situ" reaction (Figure 4a), as a reference for the following steps of the process. As already shown in Figure 3, the images of sample SILS, collected with the same voxel resolution, appear brighter than those of sample SILNS-P, in good agreement with their T_2 values (5.73 and 3.56 ms). In the figure, the SILNS sample shows a brighter region characterized by higher

spin density. This can be considered an artifact ascribable to the presence of a plug placed over the samples, used at this stage of the experiment to prevent them from moving in the tube. The artifact is due to the pressure exerted by the plug and disappears in the images of Figure 4b,c, since the plug, no more necessary, has been removed. The two bars were then swollen with perdeuterated toluene at 0 °C, in the presence of the two monomers used for the "in situ" polymerization. Images (not shown) were collected until the increasing front of toluene, which was progressively swelling the samples, vanished. Figure 4b shows the spin-echo image collected when the bars of both silicones were found to be swollen to the highest degree. Two different variables play an opposite effect on the matrix mobility and therefore on the brightness of the image contrast: the low temperature, which produces a quenching of the brightness, and the presence of the mobile solvent, which induces an enhancement of the brightness. In conclusion, the sample SILNS P is found to be brighter than it was before the onset of the "in situ" reaction (Figure 4a), but anyway darker than sample SILS. When the reaction was completed, the samples were then deswollen and brought again to room temperature As can be seen in the images of Figure 4c, the samples do not contain large agglomerates of polymer or of silica, at least at our spatial resolution, and appear quite homogeneous and similar to those collected before the onset of the reaction.

5. Conclusions

By the combination of NMRS and NMRI techniques, more complete information on the studied elastomer samples was reached.

The longitudinal relaxation time, T_1, was not significantly affected either by the change in cross-link density or by the presence of silica and/or guest polymer; the same value of T_1, in the range of the experimental error, was found for SILS, SILV, and the silicones containing the guest polymer. In agreement with the hypothesis by Garrido et al.[32] and Cuniberti,[33] the motion affecting T_1 most likely consists of a fast reorientation of the methyl group rotating around the Si−C bond, and this motion is too fast at room temperature to provide an effective contribution to T_1. On the contrary, the residual dipolar interaction affecting the transversal relaxation time was a relevant source of information. Using the Khun chain model, the transverse magnetization decay could be well described and consistently interpreted to a great extent when applied to all the examined silicones. The model gave a suitable picture of the molecular motion characteristics of the silicones investigated, allowing a connection between the cross-link density and the NMR relaxation parameters. The experimental data collected on all the elastomeric networks studied could be well fitted by eq 1 proposed in a simplified version by Khun[12] to describe the transversal magnetization decay.

On SILNS matrices whose composition was known, the A_{th} values, calculated assuming a 100% yield of the vulcanization reaction, to estimate the cross-link density, could be compared to the T_2 and qM_2 relaxation parameters fitted from the experimental data by eq 1 of the Theory section. Indeed, the T_2 and qM_2 parameters suggested that SILNS were endowed with network structures that resulted in a very good agreement with those theoretically estimated, mainly in terms of cross-link density. This result allowed to conclude that the yield of the vulcanization reaction had been similar for all samples, even if the effective yield of the reaction could not be experimentally assessed.

Two matrices SILS and SILNS P, differing for chemical composition and for the presence or the absence of a silica filler, were characterized by NMRS and NMRI experiments. The rigidifying effect of silica filler has been reported in the literature.[32] Nevertheless, SILS was found to be endowed with an intrinsic higher mobility than SILNS P, as deduced from the T_2 and qM_2 spectroscopic values and from the T_2-weighted images.

SILV, a sample obtained from SILS after an extraction procedure at 90 °C, did not give images at the voxel resolution adopted for the other samples. As suggested by the spectroscopic data, SILV is characterized by a very fast T_2 decay, incompatible with the echo time required by a spin-echo image. On the other hand, since qM_2 should not be affected by a washing procedure, it can be concluded that additional cross-links have been produced as a consequence of the high temperature used for the extraction procedure, due to an oxidative aging of the network.

An "in situ" polymerization reaction was induced in SILS and SILNS P samples at the same time and in the same NMR tube, to compare the effects of a guest polymer in terms of guest distribution and host matrix alteration in the two different silicone matrices, characterized by the presence and absence of a silica filler. The purpose was to separate the effects of the guest polymer from those of the filler. The transversal magnetization decays was not significantly affected by the presence of the guest polymer, since only a slight decrease in the T_2 value was observed in both matrices. On the other hand, qM_2 kept almost constant during the polymerization, suggesting that the "in situ" reaction did not significantly alter the silicone properties, even when performed on different matrices.

The same conclusion was also reached through the NMRI experiments since the spatial distribution of the polymer was found to be homogeneous, independent of the presence or absence of silica. Indeed, even if the spatial resolution obtained in our images was the highest achievable with our instrumentation, it was well below the silica or polymer molecular dimensions. However, it is well-known that NMRI can be sensitive to inhomogeneities well below the adopted spatial resolution. In fact, large agglomerates of polymer should create regions characterized by spatially different T_2's and hence should produce a change in the image contrast. However, as suggested by images of Figure 4, the samples are almost homogeneous. The slightly rigidifying effect observed in both matrices (shorter T_2's) was probably to be ascribed to a soft aging process occurring when the samples, after the reaction, were kept at 50 °C for 7 days to allow the toluene to evaporate.

In conclusion, by combining NMRS and NMRI techniques, a number of elastomeric matrices different in the network composition, with or without silica filler and after an extraction procedure, could be characterized.

The proposed "in situ" polymerization reaction was found to be a suitable process to be carried out on different networks and able to produce a mainly homogeneous polymer distribution, with a minor alteration of the host matrix.

Acknowledgment. The authors express their thanks to the "Fondazione Antonio de Marco" and the Italian National Research Council "Progetto Finalizzato Materiali Speciali per Tecnologie Avanzate II-Elastomeri' for financial support.

References and Notes

(1) Miller, J. B. *Prog. Nucl. Magn. Reson. Spectrosc.* **1998**, *33*, 273.
(2) Blümich, B.; Blümler, P.; Gasper, L.; Guthausen, A.; Göbbels, V.; Laukemper-Ostendorf, S.; Unseld, K.; Zimmer, G. *Macromol. Symp.* **1999**, *141*, 83.
(3) Blümler, P.; Blümich, B. *Rubber Chem. Technol. Rubber Rev.* **1997**, *70*, 468.
(4) Callagan, P. T. *Principles of Nuclear Magnetic Resonance Microscopy;* Clarendon Press: Oxford, 1991.
(5) Feio, G.; Buntix, G.; Cohen-Addad, J. P. *J. Polym. Sci., Part B: Polym. Phys.* **1989**, *27*, 1.
(6) Cory, D. G. *Solid State Nucl. Magn. Reson.* **1996**, *6*, 347.
(7) Cohen-Addad, J. P.; Vogin, R. *Phys. Rev. Lett.* **1974**, *33*, 940.
(8) Cohen-Addad, J. P.; Dupeyre, R. *Polymer* **1983**, *24*, 400.
(9) Gotlib, J. J.; Lifshitz, M. J.; Shevelev, V. A.; Lishansky, I. C.; Balanina, I. V. *Vysokomol. Soed.* **1976**, *A18*, 2299.
(10) Fedotov, V. D.; Thernov, V. M.; Khasanovitsh, T. N. *Vysokomol. Soed.* **1978**, *A20*, 919.
(11) Fedotov, V. D.; Schneider, H. Structure and Dynamics of Bulk Polymers by NMR Method. In *NMR Basic Principles and Progress;* Springer: Berlin, 1989; Vol. 21.
(12) Gronsky, W.; Hoffman, U.; Simon, G.; Wutzler, A.; Straube, E. R. *Rubber Chem. Technol.* **1992**, *65*, 63.
(13) Simon, G.; Götschmann, B.; Matzen, D.; Schneider, H. *Polym. Bull. (Berlin)* **1989**, *21*, 475.
(14) Simon, G.; Baumann, K.; Gronski, W. *Macromolecules* **1992**, *25*, 3624.
(15) Khun, W.; Barth, P.; Hafner, S.; Simon, G.; Schneider, H. *Macromolecules* **1994**, *27*, 5773.
(16) Khun, W.; Barth, P.; Denner, P.; Müller, R. *Solid State Nucl. Magn. Reson.* **1996**, *6*, 295.
(17) Knörgen, M.; Heuert, U.; Schneider, H.; Barth, P.; Khun, W. *Polym. Bull. (Berlin)* **1997**, *38*, 101.
(18) Sotta, P.; Fulber, C.; Demco, D. E.; Blumich, B.; Spiess, H. W. *Macromolecules* **1996**, *29*, 6222.
(19) Heuert, U.; Knörgen, M.; Menge, H.; Scheler, G.; Schneider, H. *Polym. Bull. (Berlin)* **1996**, *37*, 489.
(20) Chang, C.; Komoroski, R. A. *Macromolecules* **1989**, *22*, 600.
(21) Gussoni, M.; Greco, F.; Mapelli, M.; Vezzoli, A.; Ranucci, E.; Ferruti, P.; Zetta, L. *Macromolecules*, in press.
(22) Knörgen, M.; Heuert, U.; Menge, H.; Schneider, H. *Angew. Makromol. Chem.* **1998**, *261/262*, 123.
(23) Knörgen, M.; Heuert, U.; Schneider, H.; Heinrich, G. *J. Macromol. Sci., Phys.* **1999**, *B38*, 1009.
(24) Menge, H.; Hotopf, S.; Ponitzsch, S.; Richter, S.; Arndt, K.-F.; Schneider, H.; Heuert, U. *Polymer* **1999**, *40*, 5303.
(25) George, S. C.; Knörgen, M.; Thomas, S. *J. Membr. Sci.* **1999**, *163*, 1.
(26) Kuhn, W.; Grün, F. *Kolloid Z.* **1942**, *101*, 248.
(27) Abragam, A. *The Principles of Nuclear Magnetism;* Oxford University Press: Oxford, UK, 1961.
(28) Ferruti, P.; Ranucci, E. *Makromol. Chem. Rapid Commun.* **1987**, *8*, 549.
(29) Ranucci, E.; Ferruti, P.; Neri, M. G. *J. Bioact. Compatible Polym.* **1989**, *4*, 403.
(30) Ranucci, E.; Ferruti, P.; Neri, M. G. *J. Biomater. Sci. Polym. Ed.* **1991**, *2*, 255.
(31) Ranucci, E.; Ferruti, P.; Della Volpe, C.; Migliaresi, C. *Polymer* **1994**, *35*, 5571.
(32) Garrido, L.; Mark, J. E.; Sun, C. C.; Ackerman, L. J.; Chang, C. *Macromolecules* **1991**, *24*, 4067.
(33) Cuniberti, C. *J. Polym. Sci.* **1970**, *8*, 2051.

MA011356D